Supporting information

A crystalline-amorphous interface engineering in Fe-doped Ni_xP electrocatalyst for highly efficient oxygen evolution reaction

Shuai Cao[1], Xiaoming Fan[2,3,*], Li Wei[2,3],Ting Cai[2,3], Yuping Lin[2,3], and Zeheng Yang[2,3,*]

[1] Traditional Chinese Medicine College, Bozhou University, 236800 Bozhou, Anhui, PR China

[2] School of Chemistry and Chemical Engineering, Hefei University of Technology, 230009 Hefei, Anhui, PR China

[3] Anhui Province Key Laboratory of Advanced Catalytic Materials and Reaction Engineering, 230009 Hefei, Anhui, PR China

* Corresponding authors

E-mail: xmfan@hfut.edu.cn (Xiaoming Fan), zehengyang@hfut.edu.cn (Zeheng Yang)

Experimental section

Materials

$Fe(NO_3)_3 \cdot 9H_2O$ (≥98.5%), urea (≥99%), $NaH_2PO_2 \cdot H_2O$ (98%-103%), RuO_2 (99.9%), and 20 wt% Pt/C were obtained from Sinopharm Chemical Reagent Co., Ltd. The Ni foam was purchased from Shenzhen Meisen electromechanical equipment Co., Ltd. The water used in this study was purified via a Millipore system. All chemicals were used as received without further purification.

Synthesis of Fe-Ni_xP/NF

The NiFe-LDH/NF composite was prepared via a hydrothermal reaction. In detail, 10 mmol of urea was dissolved in 36 mL $Fe(NO_3)_3$ solution (5.56 mM). The homogeneous solution was then transferred into a 50 mL Teflon-lined stainless-steel autoclave. Ni foam substrates (2 × 4 cm^2) were carefully washed with HCl solution (3.0 M) and then rinsed with absolute ethanol and deionized water. After immersing a washed Ni foam substrate in the homogeneous solution, the autoclave was sealed and maintained at 100 ^oC for 3 h and then naturally cooled down to room temperature. The array sample grown on Ni foam was collected and rinsed with absolute ethanol and deionized water several times and dried at 60 °C in air for 12 h.

The as-prepared NiFe-LDH/NF were immersed in 0.1 M of KOH solution in the 50 mL Teflon-lined stainless-steel autoclave, and the autoclave was sealed and maintained at 120 ^oC for 5 h and then naturally cooled down to room temperature. The derived NiFe-based arrays (denoted as NiFe-LDH-T/NF) were rinsed several times by deionized water and dried at 60 °C for 12 h for next step transformation. The

NiFe-LDH-T/NF were further modified through phosphatization with $NaH_2PO_2 \cdot H_2O$, which was conducted in two stacked ceramic boats with $NaH_2PO_2 \cdot H_2O$ powder in the big boat on the upstream side and the NiFe-based arrays in the small boat at the downstream of the tube furnace. The ceramic boats were heated to 300 °C in a temperature-programmed tube furnace at a ramp rate of 5 °C min^{-1} in a N_2 gas flow and maintained at 300 °C for 3 h.

Synthesis of Fe-Ni_xP-N/NF

In detail, 10 mmol of urea was dissolved in 36 mL $Fe(NO_3)_3$ solution (5.56 mM). The homogeneous solution was then transferred into a 50 mL Teflon-lined stainless-steel autoclave. Ni foam substrates (2 × 4 cm^2) were carefully washed with HCl solution (3.0 M) and then rinsed with absolute ethanol and deionized water. After immersing in a washed Ni foam substrate in the homogeneous solution, the autoclave was sealed and maintained at 100 ºC for 3 h and then naturally cooled down to room temperature. The array sample was collected and rinsed with absolute ethanol and deionized water several times and dried at 60 °C in air for 12 h.

The NiFe-LDH/NF were further modified through phosphatization with $NaH_2PO_2 \cdot H_2O$, which was conducted in two stacked ceramic boats with $NaH_2PO_2 \cdot H_2O$ powder in the big boat on the upstream side and the NiFe-LDH/NF in the small boat at the downstream of the tube furnace. The ceramic boats were heated to 300 °C in a temperature-programmed tube furnace at a ramp rate of 5 °C min^{-1} in a N_2 gas flow and maintained at 300 °C for 3 h.

Fabrication of RuO_2/NF and Pt/C/NF electrodes

For comparison, the activity of RuO_2 was evaluated. The working electrode of the commercial catalyst was prepared by ultrasonicating RuO_2 and 20 wt% Pt/C powder in ethanol with a Nafion ionomer (Sigma-Aldrich) for 1 h to obtain a homogeneous slurry, then casting the catalyst slurry on a piece of NF (1 cm × 1 cm).

Material Characterization

Powder X-ray diffraction (XRD) patterns were obtained using an X-ray diffractometer by using a Cu Kα radiation source (λ= 0.154178 nm) performed at 40 kV and 80 mA (X'PERT PRO, Panalytical). The morphologies of the samples were analyzed by scanning electron microscope (SEM, Hitachi SU8020) and transmission electron microscope (TEM, JEOL JEM-2100F). An X-ray photoelectron spectrometer (XPS, Thermo Fisher Scientific ESCALAB250Xi) was used for testing the surface element composition and valence state of the as-synthesized samples.

Electrochemical Measurement

The OER tests were performed with a Chenhua CHI 760E electrochemical analyzer. All electrochemical measurements were conducted in a standard three-electrode system with a Pt foil as the counter electrode, Hg/HgO as the reference electrode, and the self-supporting arrays grown on Ni foam (1 × 1 cm^2) as the working electrode. Before the electrochemical measurements were conducted, 1.0 M KOH solution was purged with O_2 (OER tests) for 30 min. After several cyclic voltammetry tests with a

scan rate of 5 mV s^{-1} to get stable curves, linear sweep voltammetry (LSV) for OER was performed at a scanning rate of 5 mV s^{-1}. The corresponding polarization curves presented were all calibrated after iR correction. The current density was normalized to the geometrical area, and potentials versus Hg/HgO were converted to versus RHE (reversible hydrogen electrode) according to the Nernst equation ($E_{RHE} = E_{Hg/HgO} + 0.059 \times pH + 0.098$). The Tafel slope was calculated according to the following formula：

$$\eta = b\log(j/j_o)$$

where η is the overpotential, b is the Tafel slope, j is the current density, and j_o is the exchange current density. Electrochemical impedance spectroscopy (EIS) was performed from 0.01 Hz to 100 kHz at the open circuit potential. Polarization curves were obtained using LSV with a scan rate of 5 mV s^{-1}. The long-term durability test was performed using constant current electrolysis. The electrodes with a geometric area of 0.4 cm × 0.5 cm were used to measure the stability at 500 mA cm^{-2} and 1000 mA cm^{-2} current densities, respectively, when the current was set to 0.1 and 0.2 A. All experiments were carried out at room temperature (~25 ^{o}C).

Figure S1

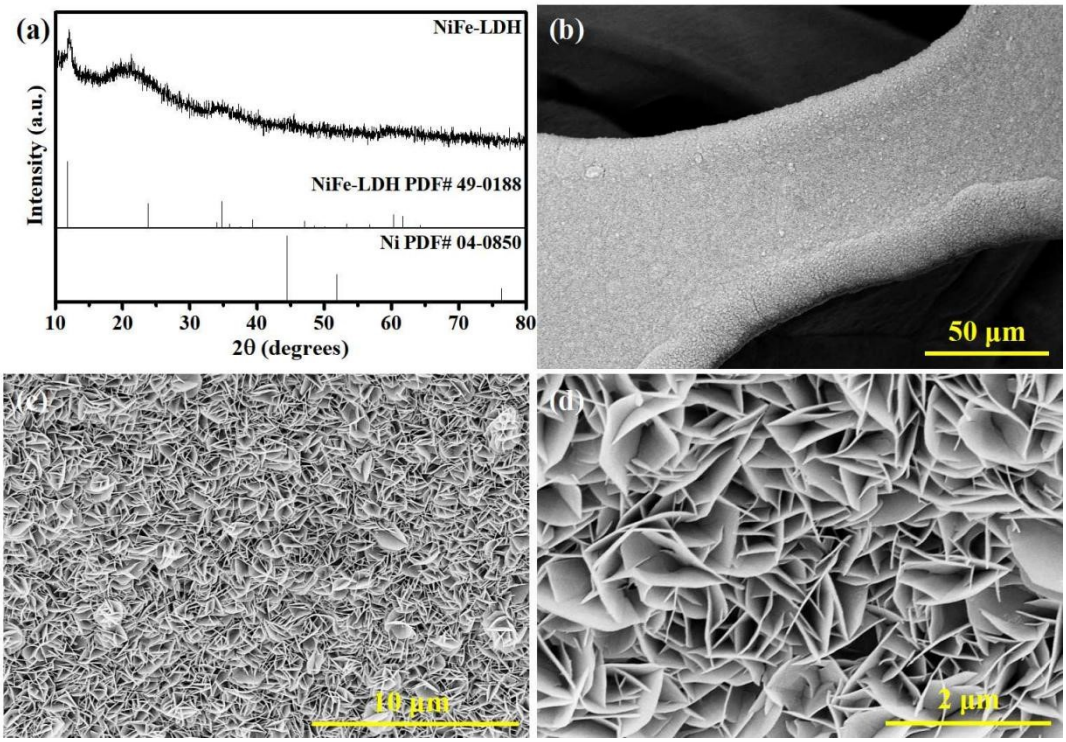

Figure S1. XRD pattern (a) of the NiFe-LDH and typical SEM images (b-d) of the NiFe-LDH/NF.

Figure S2

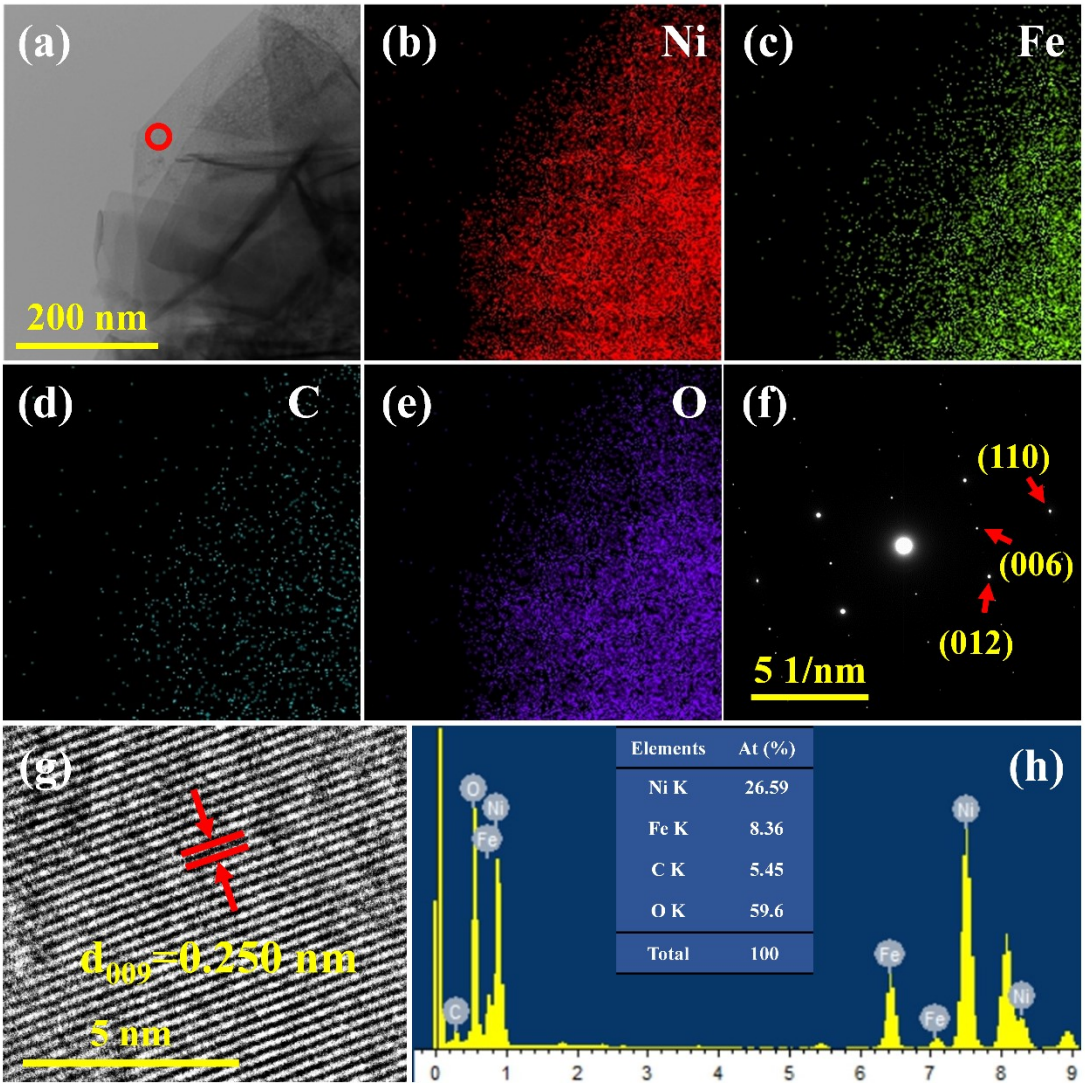

Figure S2. (a) TEM image, the elemental mapping images of Ni (b), Fe (c), C (d) and (e) O, (f) SAED pattern, (g) HRTEM image and (h) energy dispersive spectra of the NiFe-LDH.

Figure S3

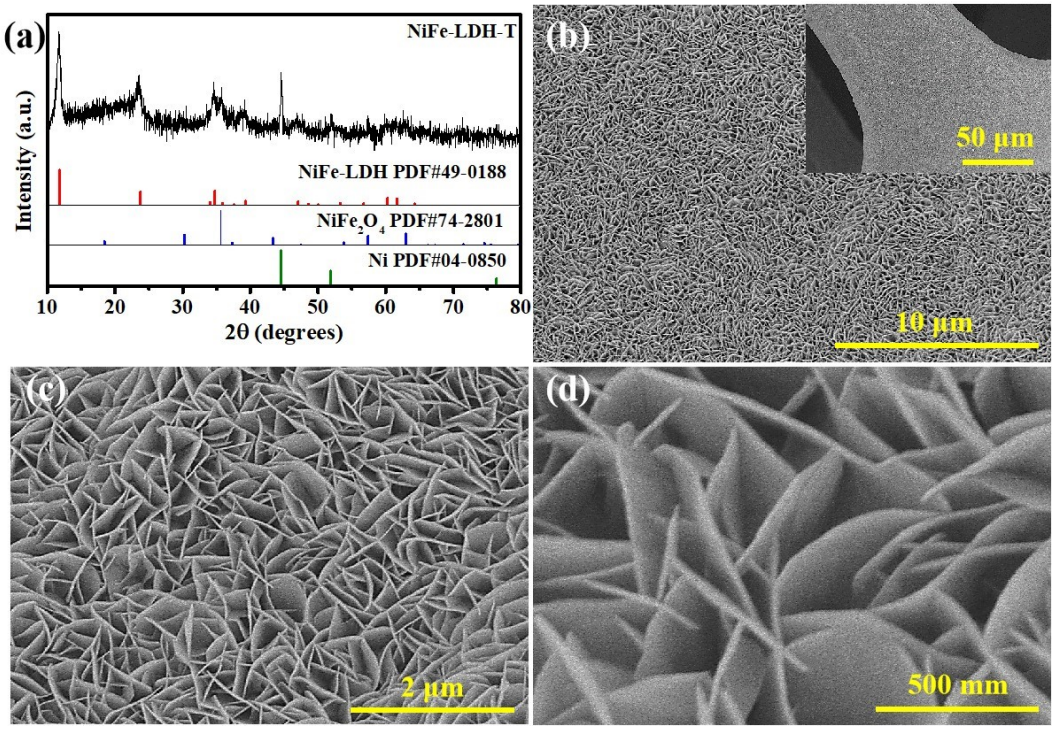

Figure S3. (a) XRD pattern of the NiFe-LDH-T. (b-d) Typical SEM images of the NiFe-LDH-T/NF.

Figure S4

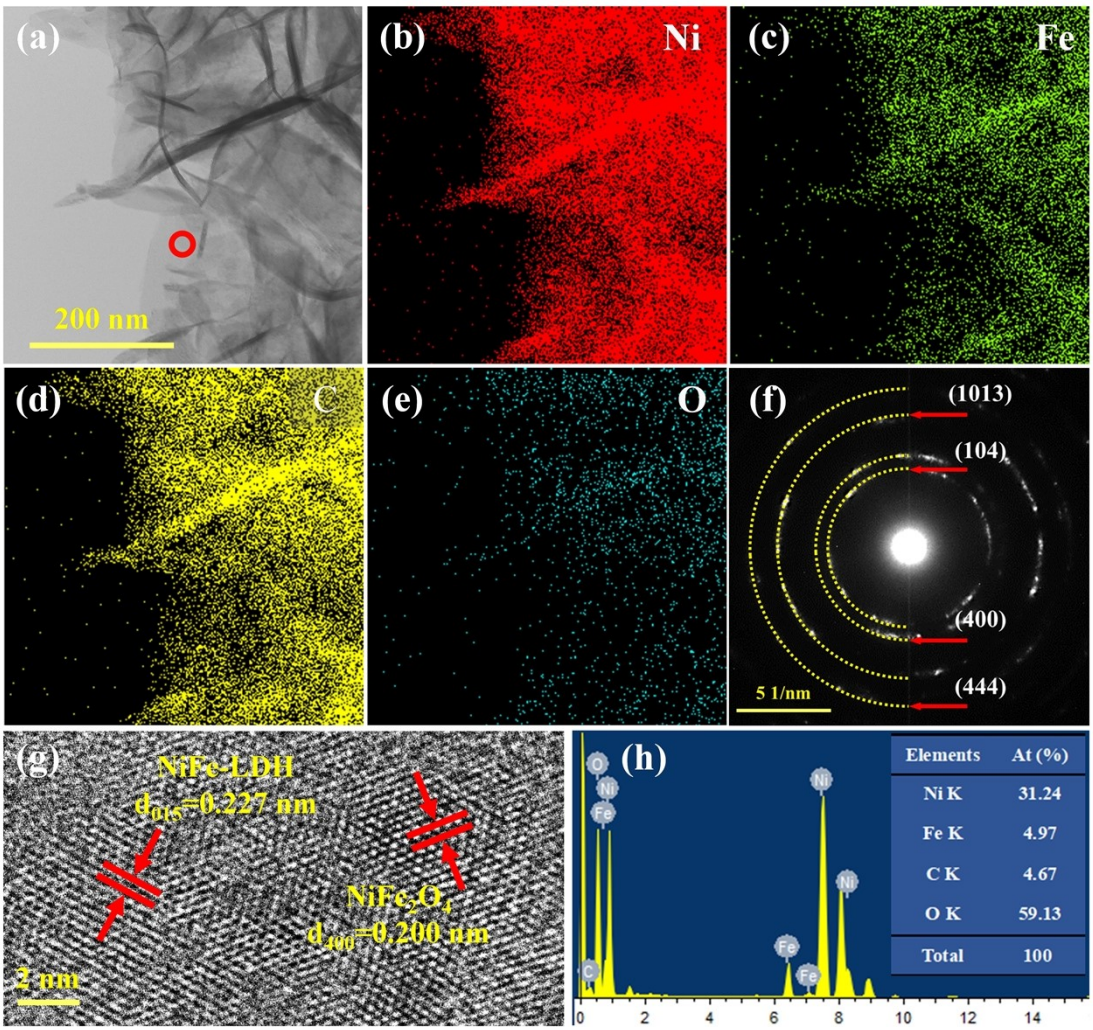

Figure S4. (a) TEM image, the elemental mapping images of Ni (b), Fe (c), C (d) and (e) O, (f) SAED pattern, (g) HRTEM image and (h) energy dispersive spectra of the NiFe-LDH-T.

Figure S5

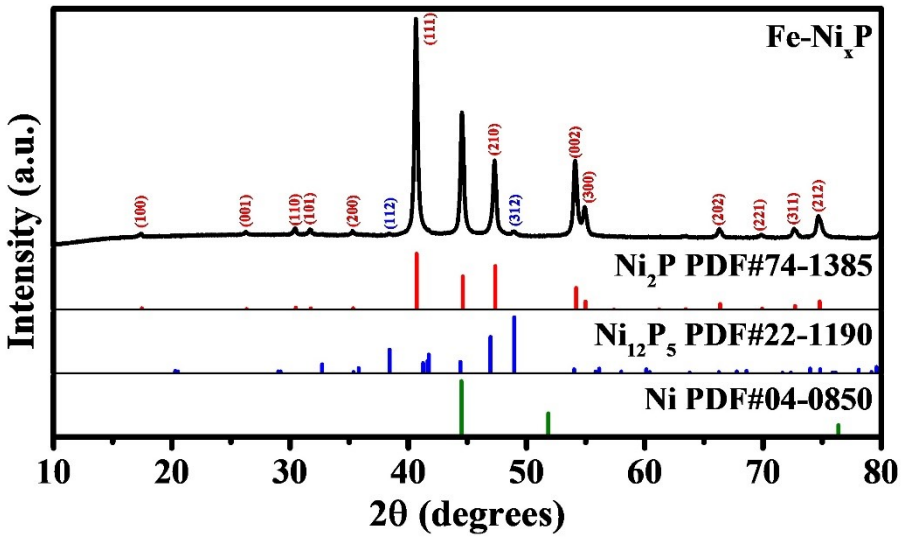

Figure S5. XRD pattern of the Fe-Ni$_x$P.

Figure S6

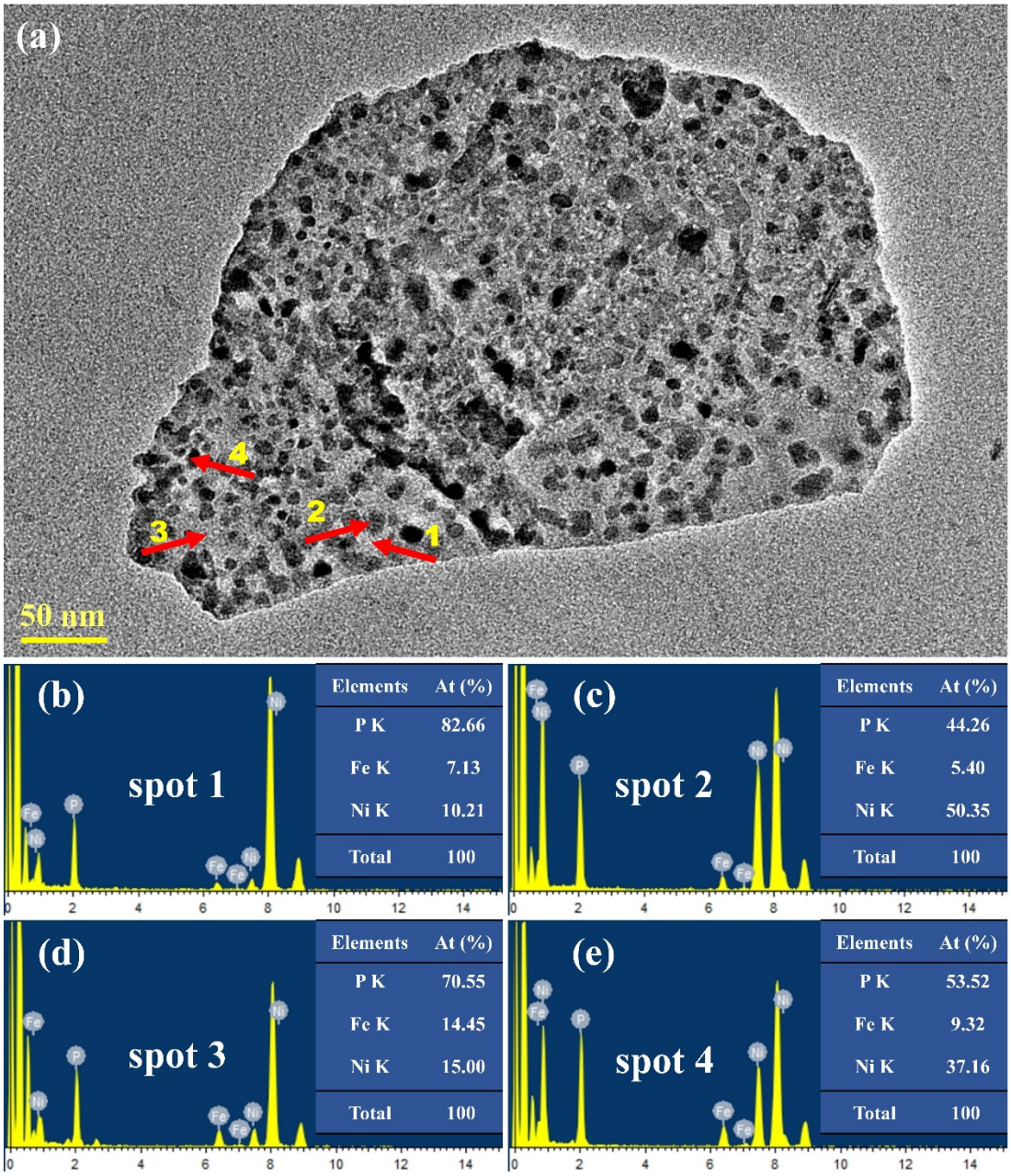

Figure S6. (a) The high-magnification TEM image of the the Fe-Ni_xP nanosheet. (b-e) Energy dispersive spectra of the different locations for the Fe-Ni_xP nanosheet.

EDS spectra (Figure S6b-e) were performed for the positions of different shades and colors pointed to by the arrows (inset of Figure S6a). The atomic ratios of Ni:Fe:P in light amorphous region marked in 1 and 3 of the Figure S6a were 10.21:7.13:82.66 and 15.00:14.45:70.55, and the atomic ratios in dark polycrystalline region marked in

2 and 4 of the Figure S6a were 50.35:5.4:44.26 and 37.16:9.32:53.52, respectively. The difference of atomic ratio of elements in different regions further proves the existence of sample shrinkage after phosphating. As can be seen from the above ratios, the percentage content of Fe in the dark polycrystalline region is lower than that in the light area, while the percentage content of Ni is higher than that in the light amorphous region, which may be caused by the different thermal contraction rates of Ni and Fe elements.

Figure S7

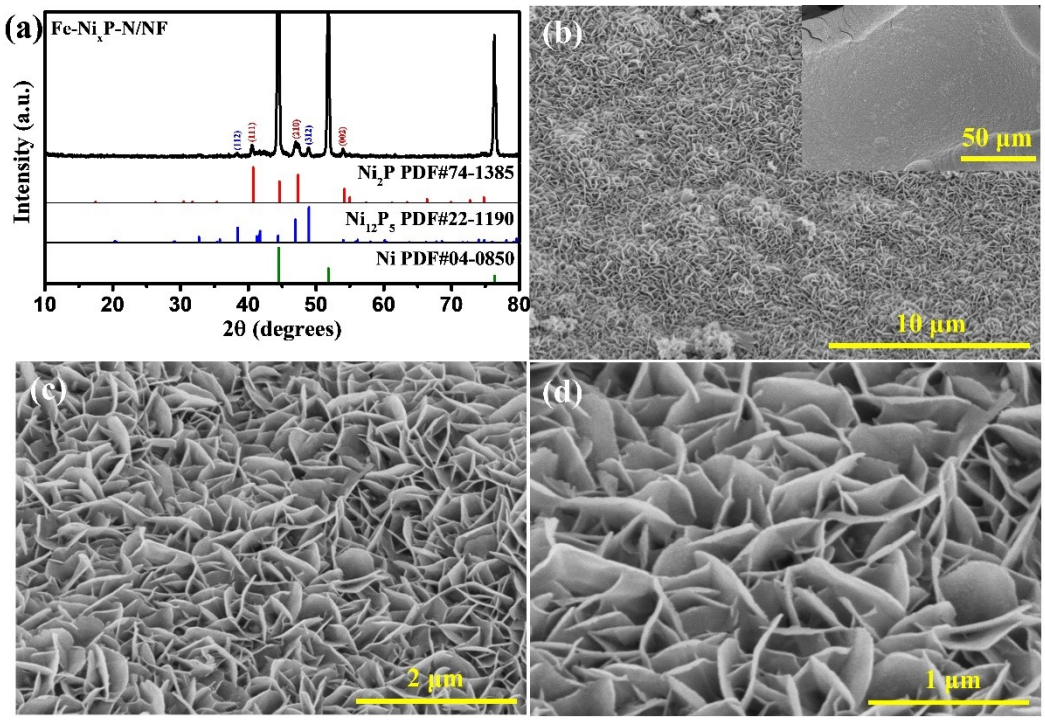

Figure S7. XRD pattern (a) and typical SEM images (b-d) of the Fe-Ni$_x$P-N/NF.

To explore the effects of alkali treatment, the composition and morphology of the Fe-Ni$_x$P-N/NF were investigated. The X-ray diffraction patterns in Figure S7a is not intense but still show that Ni_2P (PDF No. 74-1385) and $Ni_{12}P_5$ (PDF No. 22-1190) are obtained after phosphidation. In Figure S7a, the peaks in the XRD patterns located at 44.34, 51.74 and 76.24° are attributed to the Ni foam substrate. The SEM image of Fe-Ni$_x$P-N/NF shows that Ni foam is entirely covered with uniform nanosheets (Figure S7b-d).

Figure S8

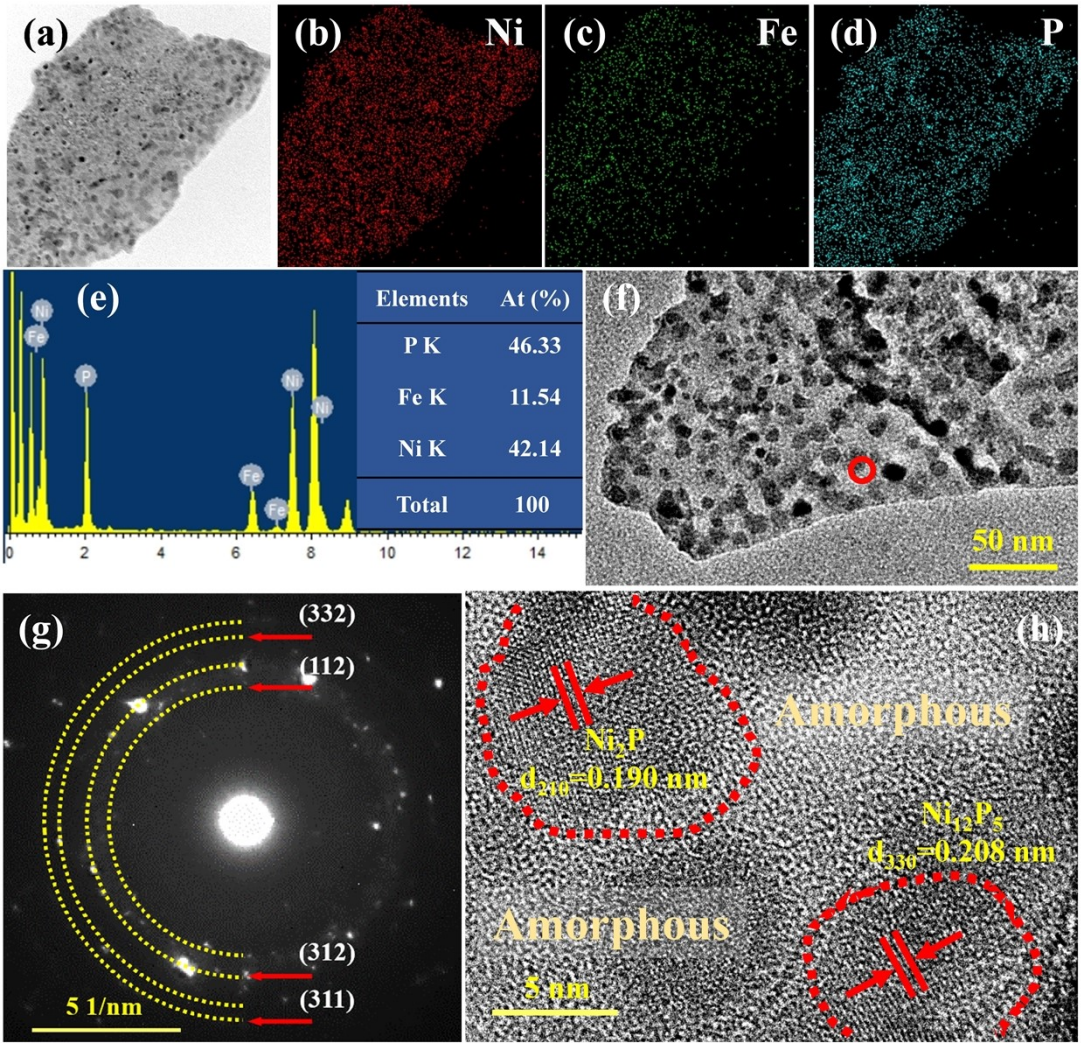

Figure S8. (a, f) TEM images, the elemental mapping images of Ni (b), Fe (c) and P (d), (e) energy dispersive spectra, (g) SAED pattern and (h) HRTEM image of the Fe-Ni_xP-N.

Figure S9

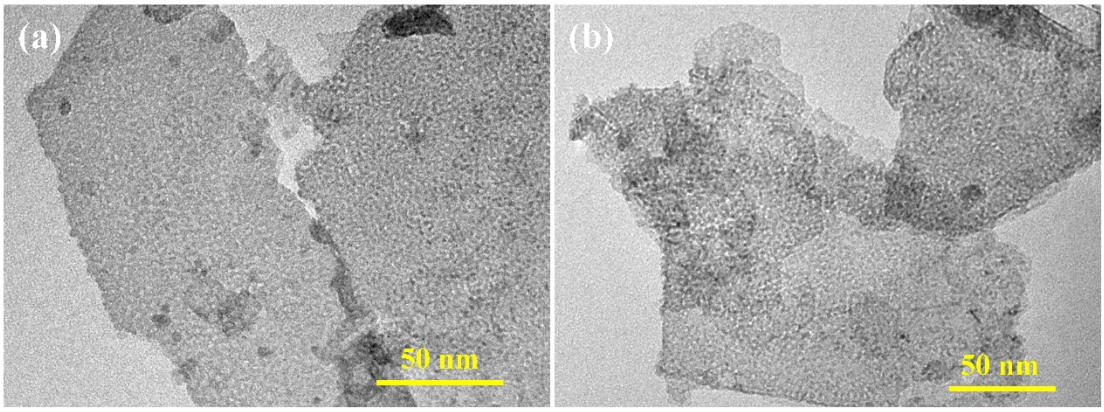

Figure S9. TEM image of NiFe-LDH (a) and NiFe-LDH-T (b) which were heated in a temperature-programmed tube furnace at a ramp rate of 5 °C min^{-1} in a N_2 gas flow and maintained at 300 °C for 3 h.

Figure S10

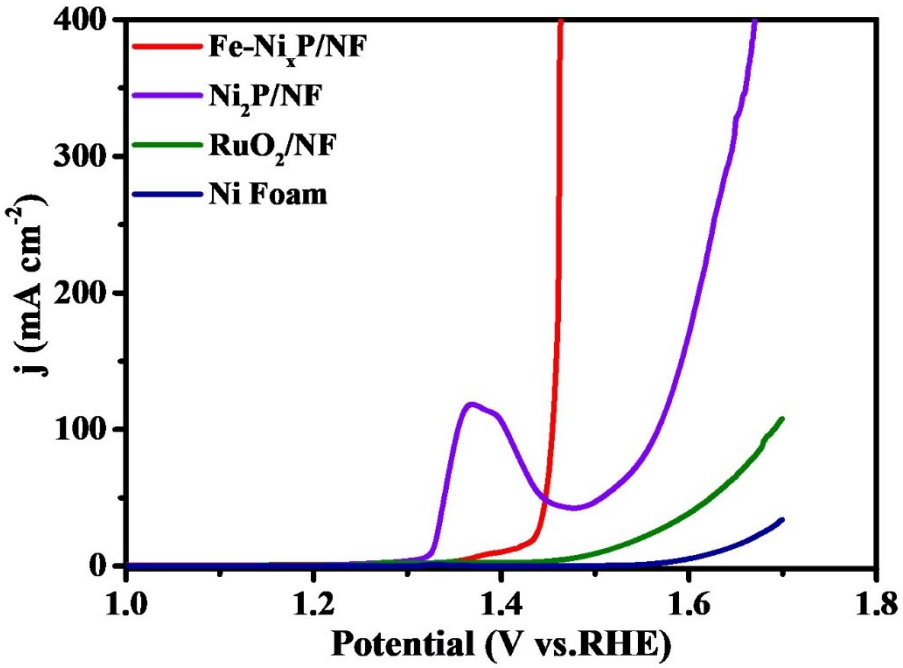

Figure S10. (a) Polarization curves for OER (iR-corrected) of the samples.

Ni_2P/NF was prepared by referring to the literature (*Inorg. Chem.* **2019**, *58*, 11630−11635).

Figure S11

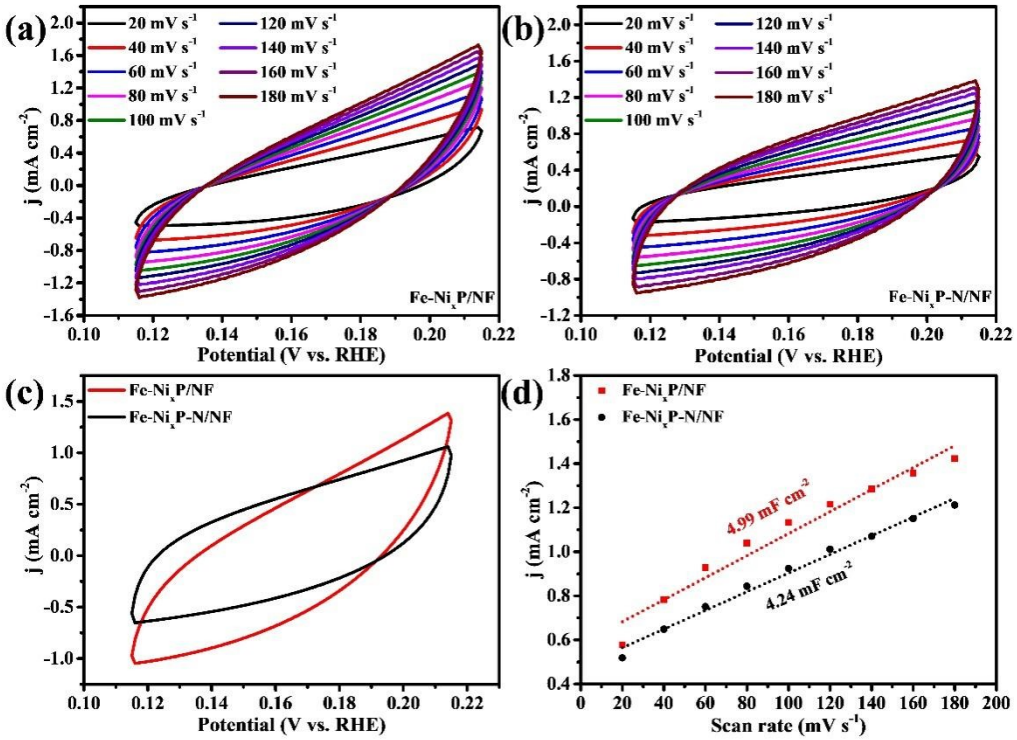

Figure 11. CVs of (a) Fe-Ni_xP/NF and (b) Fe-Ni_xP-N/NF in the non-faradaic capacitance current range at different scanning rates. (c) CV curves of the samples at 100 mV s^{-1}. (d) The linear dependence of capacitive current at 0.2 V vs. RHE on the scan rate for Fe-Ni_xP/NF and Fe-Ni_xP-N/NF.

Figure S12

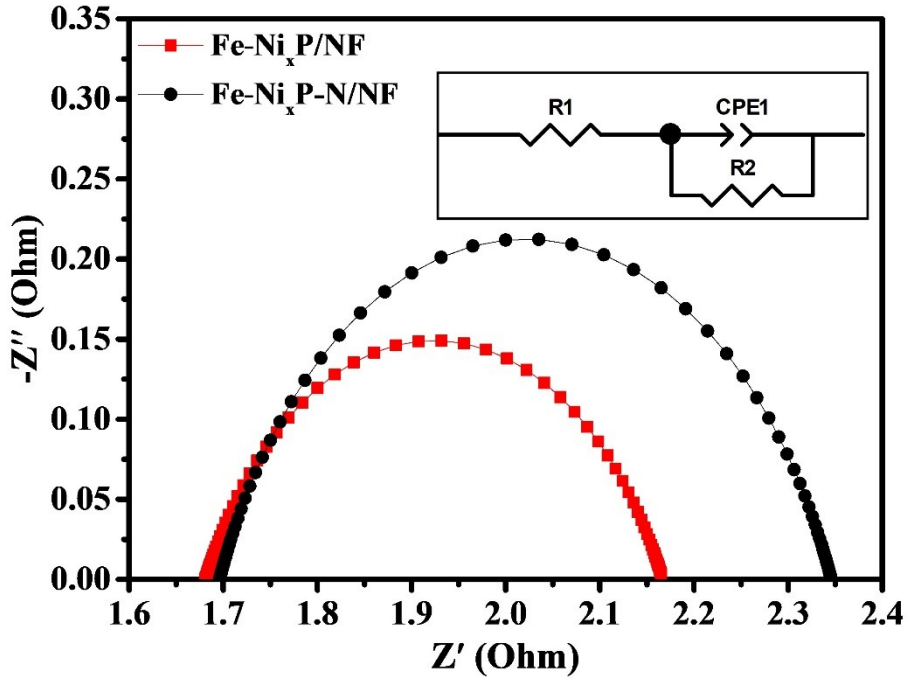

Figure S12. Nyquist plots of the samples. Inset: the corresponding equivalent circuit diagram consisting of an electrolyte resistance (R_1), a charge-transfer resistance (R_2), and a constant-phase element (CPE).

The kinetics of the catalyst at the electrode/electrolyte interface was studied by electrochemical impedance spectroscopy (EIS) as shown in Figure S12. All EIS data are equipped with an equivalent circuit as shown inset of the Figure S12, including a resistor (R_1) in series, a resistor (R_2) and a parallel combination of a constant phase (CPE1) element. In the equivalent circuit, R_1 is the ohmic resistance of electrolyte, electrocatalyst and all contacts, and R_2 is the charge transfer resistance between catalyst and electrolyte. The lower the R_2 value, the faster the reaction rate. According to the results of the installation EIS (Table S2, supporting information), Fe-Ni$_x$P/NF exhibits the smallest R_2 (0.49 Ω), indicating rapid charge transfer kinetics. This is related to the low overpotential and the small Tafel slope for the Fe-Ni$_x$P/NF.

Figure S13

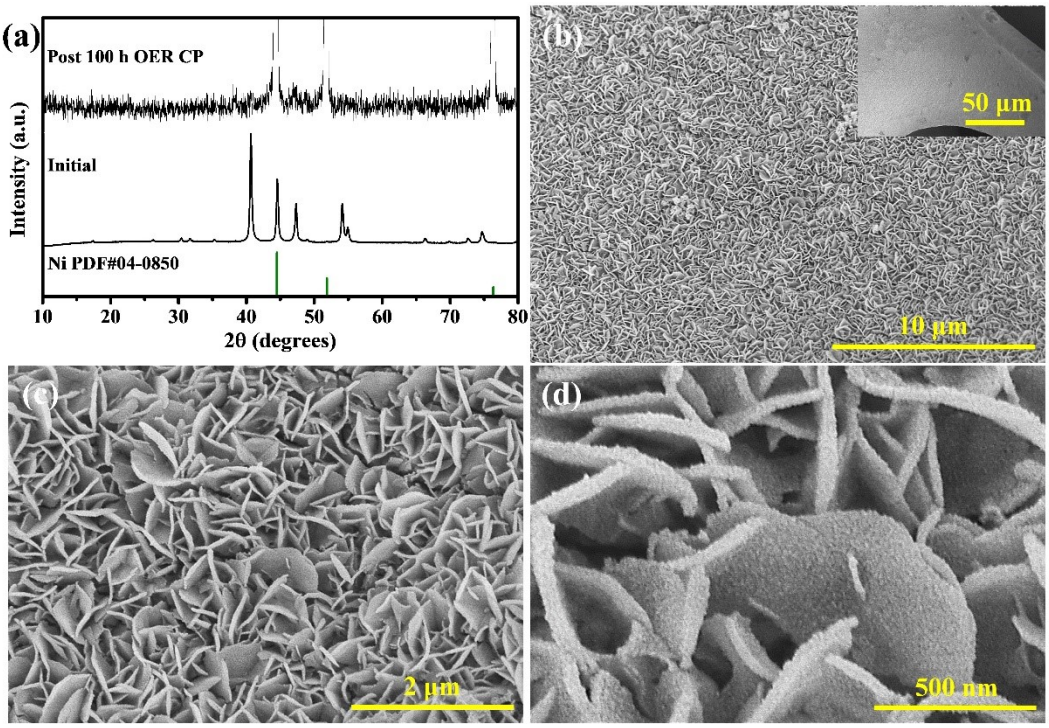

Figure S13. (a) XRD pattern and (b-d) SEM images of Fe-Ni_xP/NF after 100 h CP test for OER.

Figure S14

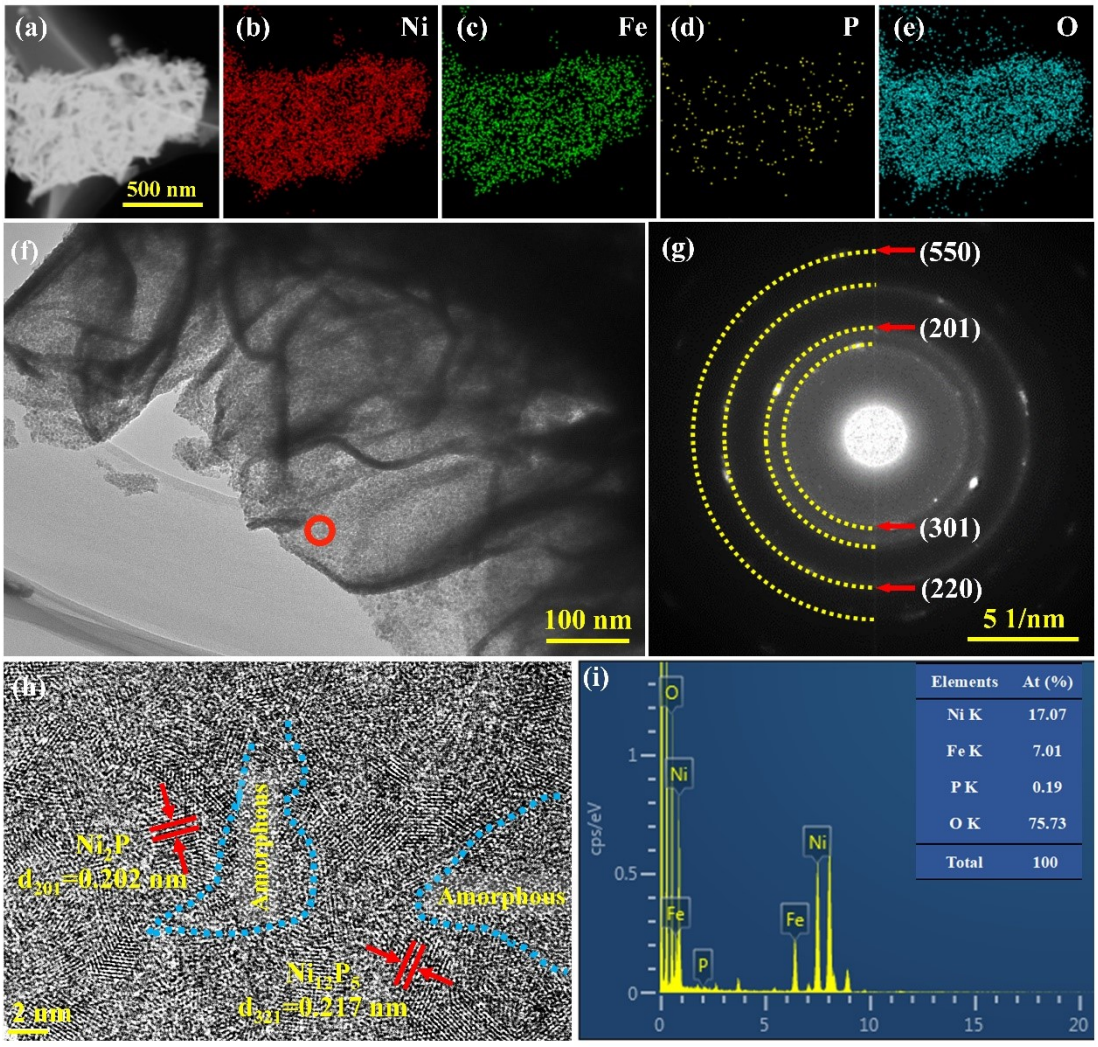

Figure S14. Morphology characterizations of Fe-Ni_xP after stability testing. (a) the low-magnification TEM image and (b-e) the corresponding elemental mapping images. (f) the high-magnification TEM image. (g) SAED pattern, (h) HRTEM image, and (i) EDS spectrum of Fe-Ni_xP after 100 h CP test for OER.

Figure S15

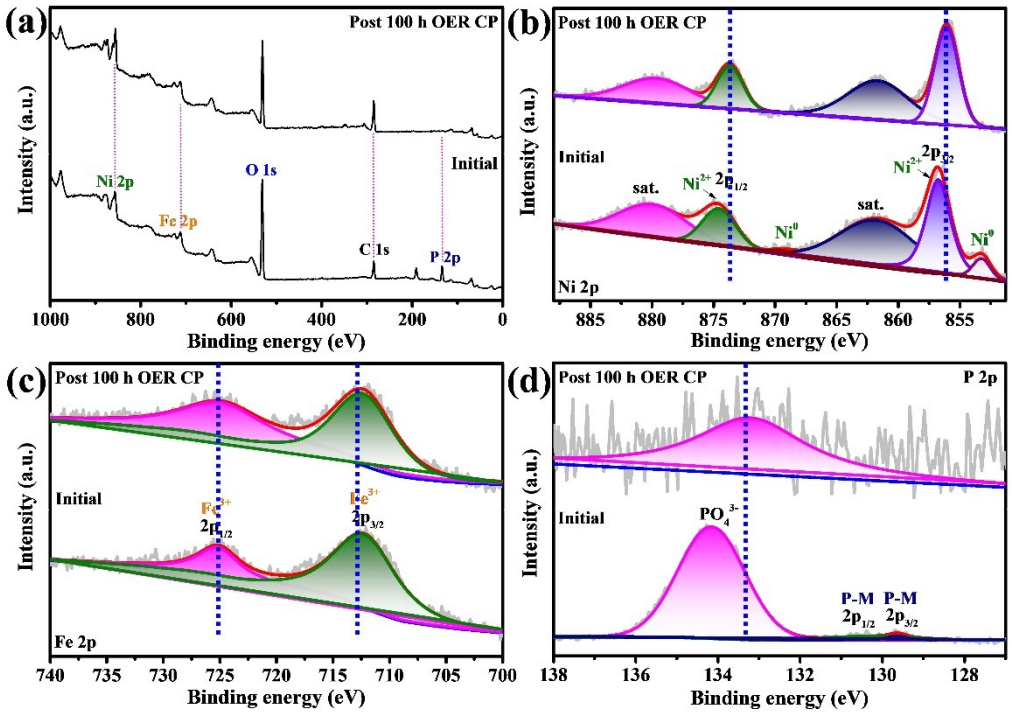

Figure S15. XPS spectra of Fe-Ni_xP/NF before (down) and after (up) stability testing.

Table S1 Recently reported non-precious metal OER electrocatalysts in alkaline media

Catalyst	j (mA cm^{-2})	Overpotential (mV)	Tafel slope (mV dec^{-1})	Electrolyte	Reference
	20	**204**			
Fe-Ni_xP/NF	**100**	**225**	**25**	**1.0 M KOH**	**This work**
	300	**231**			
NiFeP/CoP/NF	20	250	51	1.0 M KOH	*Int. J. Hydrogen Energy*, 2019, **44**, 19986-19994
NiFeP/SG	10	218	44	1.0 M KOH	*Nano Energy*, 2019, **58**, 870-876
$NiFeO_x$/NiFeP/NF	100	320	57.9	1.0 M KOH	*Int. J. Hydrogen Energy*, 2019, **44**, 26118-26127
Mn-Ni_2P/NF	100	330	116.7	1.0 M KOH	*Catal. Today*, 2020, **355**, 815-821
Fe-doped Ni_2P/C	10	205	52	1.0 M KOH	*ACS Catal.*, 2019, **9**, 8882-8892
$(Ni_xFe_{1-x})_2P$	150	300	59.3	1.0 M KOH	*ACS Catal.*, 2020, **10**, 9086-9097
FeP/CeO_2–NF	100	245	39.1	1.0 M KOH	*Chem. Commun.* 2020, **56**, 4228-4231
P-$(Ni,Fe)_3S_2$	100	246	30	1.0 M KOH	*ACS Appl. Mater. Interfaces*, 2019, **11**, 27667-27676

P-NiFe	100	230	32	1.0 M KOH	*Chem. Sci.*, 2018, **9**, 1375-1384
a-NiFe-OH/NiFeP/NF	300	258	39	1.0 M KOH	*ACS Energy Lett.*, 2017, **2**, 1035-1042

Table S2 Summary of the EIS results fitted to the equivalent circuit board

Sample	R_1	R_2
Fe-Ni_xP/NF	1.68	0.49
Fe-Ni_xP-N/NF	1.69	0.65